# Input Impedance, Nanocircuit Loading, and Radiation Tuning of Optical Nanoantennas

Andrea Alù, and Nader Engheta[*]

Dept. of Electrical and Systems Engineering

University of Pennsylvania

Philadelphia, PA 19104, U.S.A.

**Abstract**

Here we explore the radiation features of optical nanoantennas, analyzing the concepts of input impedance, optical radiation resistance, impedance matching and loading of plasmonic nanodipoles. We discuss how the concept of antenna impedance may be applied to optical frequencies, and how its quantity may be properly defined and evaluated. We exploit these concepts in optimization of nanoantenna loading by optical nanocircuit elements, extending classic concepts of radio-frequency antenna theory to the visible regime for the proper design and matching of plasmonic nanoantennas.

PACS numbers:78.67.-n, 84.40.Ba, 73.20.Mf, 68.37.Uv

---

[*] To whom correspondence should be addressed.  E-mail: engheta@ee.upenn.edu

The anomalous electromagnetic features of plasmonic materials and components at optical frequencies have been recently applied to various fields, and in particular to the realization of optical devices with reduced size and enhanced functionalities The research is currently leading towards the realization of integrated plasmonic devices that may have functionalities similar to their radio-frequency (RF) counterparts, but with much enhanced bandwidth, speed and compactness. This interest has been accompanied by remarkable advancements in nanotechnology, fabrication and measurement of nanostructures with the desired geometry and electromagnetic properties in the nanometer scales.

Driven by these advancements, and in particular by the possibility of realizing plasmonic nanorods with elongated shapes and relatively high aspect ratios, several groups have experimentally investigated the realization of nanoantennas in the form of monopole and dipole antennas made of plasmonic materials [1]-[6]. From a theoretical point of view, however, the recipe for proper design and performance optimization of these nanoradiators is still in its embryonic stage when compared with well-known design methods for conventional RF antennas. A recent letter [7] has pointed out the shortening of the effective wavelength "seen" by the plasmonic dipole with respect to the free-space wavelength, consistent with the well known slow-wave properties of plasmonic nanorods [8]. All such studies, however, have been concerned with the scattering properties of these components when illuminated by external sources, e.g., light beams or microscope tips, or with their interaction with nanostructures nearby. It is interesting to note however that, by definition, one of the main functions of any

antenna includes 'connecting' and 'matching' a source, a receiver, or a waveguide to the 'outside' region (e.g., free space domain) in order to transmit (or receive) a given signal to (or from) the far field. In this sense, the concepts of input impedance at the feeding point, antenna's radiation resistance, and the role of loading an antenna, all of which are familiar notions for traditional RF antennas, are quantities of fundamental importance for a proper design and use of antennas. These parameters, however, cannot be obtained from the scattering analysis. This is why, for instance, in [9] a simplified transmission-line analysis has been applied to the conduction current distribution over a carbon nanotube, deriving to first approximation its radiation properties, and pointing out some potentially important differences between RF and higher-frequency dipoles.

In this letter we transplant the concepts of input impedance, radiation resistance, loading and impedance matching into the optical domain, and we investigate them for plasmonic nanoantennas in the form of plasmonic nanodipoles. These results may lead to a paradigm for bringing the classical antenna concepts from RF to optical frequencies, in order to facilitate a realistic design and use of such nanodevices as efficient radiating or receiving optical elements at nanoscales for potential applications in telecommunications, super-resolution microscopy, biological and medical optical sensing.

The geometry of the problem is depicted in Fig. 1, which consists of a cylindrical nanodipole of total length $L$ and radius $R$, made from silver, and terminated on both sides by spherical tips. The dipole is assumed to be fed at its center gap of thickness $g$. This resembles a conventional center-fed RF dipole antenna;

however, here the optical nanoantenna is made of silver, a low-loss noble metal whose permittivity in the IR and optical regime may be described as a classic Drude model $\varepsilon_{Ag} = \varepsilon_0 \left[ \varepsilon_\infty - f_p^2 / \left( f \left( f + i\gamma \right) \right) \right]$ with $\varepsilon_\infty = 5$, $f_p = 2.175\,PHz$ and $\gamma = 4.35\,THz$ [10].
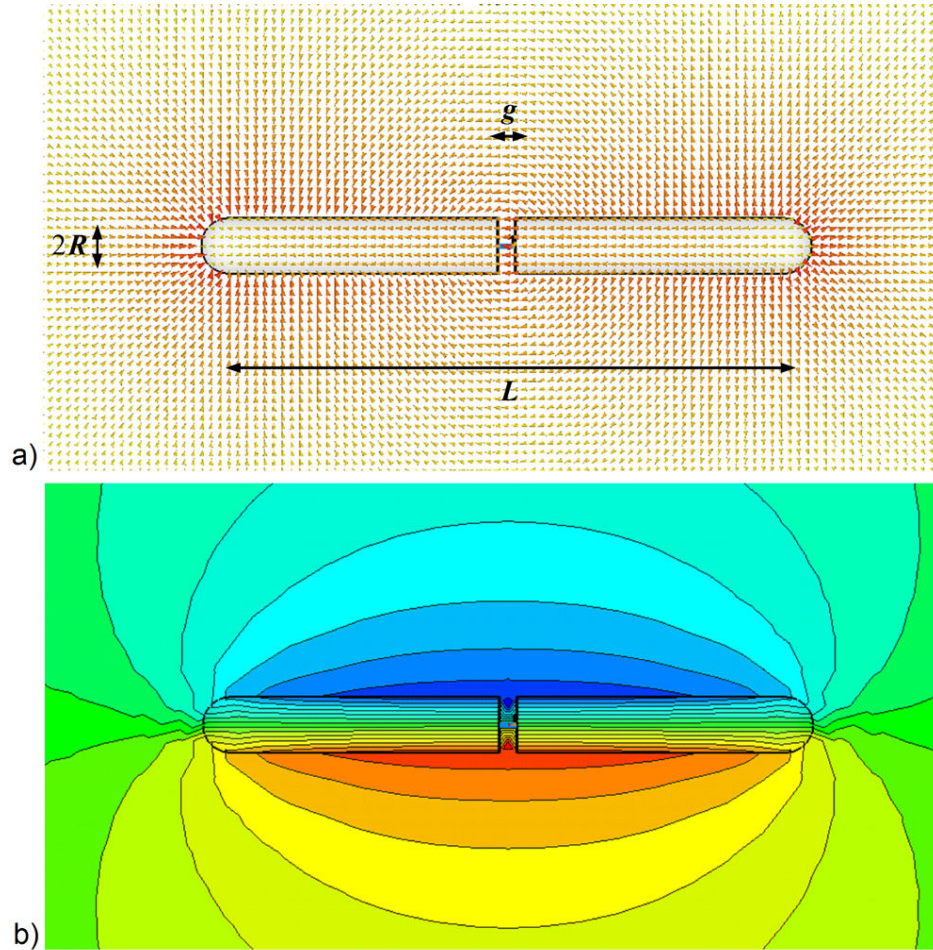


Figure 1 – (Color online) Geometry and (s) electric and (b) magnetic field distributions on the E plane (snapshots in time) at the resonant frequency for which $L \simeq \lambda_{eff} / 2$ for a silver nanodipole antenna. In this case, $L = 110\,nm$ and $f = 266\,THz$. Brighter colors and longer arrows correspond to stronger values of the field.

Feeding the nanoantenna at its gap allows one to determine its input impedance $Z_{in} = R_{in} - iX_{in}$, defined as the ratio of the driving optical voltage difference across the gap to the total flux of induced optical displacement current flowing from the feeding source into the antenna (and the gap). Figs. 2a and 2b report $R_{in}$ (resistive component) and $X_{in}$ (reactive component) for different lengths of the nanodipole, while $R = 5\,nm$ and $g = 3\,nm$ kept fixed, using full-wave time-domain simulation software [11]. For very low frequencies, the silver is a conductive metal and the corresponding impedance is strongly capacitive (i.e., $X_{in} < 0$), analogous to a short RF dipole. However, increasing the frequency up to the IR and visible regime, the plasmonic features of silver come into play and the antenna hits its first resonance at the frequency for which $X_{in} = 0$, indicated, as an example, by the blue arrow in Fig. 2b for the $L = 160\,nm$ curve. It is evident that by decreasing the length $L$, the antenna resonant frequency shifts up, analogous to the case of a regular RF dipole. Its position is located around the frequency for which the condition $L = \lambda_{eff} / 2$ holds, where $\lambda_{eff}$ is the effective wavelength "seen" by the plasmonic dipole, which is shorter than the free-space wavelength $\lambda_0$, and it may be determined with good approximation as the wavelength of the guided $TM_{10}$ mode supported by an infinite silver nanorod of raidus $R$, yielding results consistent with the approximate linear formula derived in [7]. The value of the input resistance at this resonance frequency is lower than that of a regular RF dipole antenna (for instance $R_{in} = 22.2\,\Omega$ for the dipole of Fig. 1 with $L = 110\,nm$), as discussed in the following. Consistent with the

5

transmission-line model of a dipole [12], this first resonance has a low input impedance, and it may be seen as a "short-circuit" resonance (i.e., $X_{in} = 0$) associated with the condition $L = \lambda_{eff} / 2$. In contrast, a sharp "open-circuit" resonance (i.e., where $R_{in}$ and $X_{in}$ very large) is also noticed in Fig. 2 at a somewhat higher frequency, which corresponds to the sharp impedance resonance in the plots. The impedance values associated with this resonance here are larger than those obtained at the $L = \lambda_0$ resonance for a regular conducting RF dipole antenna with similar aspect ratio, owing to the plasmonic properties of the nanoantenna. Moreover, the "open-circuit" resonant frequency is lower than the $L = \lambda_{eff}$ frequency, due to the non-negligible capacitance of the air gap region. The input impedance evaluated in Fig. 2 may indeed be regarded as the parallel combination of the "intrinsic" impedance of the nanodipole $Z_{dip}$ and the air gap capacitive impedance $Z_{gap}$. This is consistent with the circuit model depicted in the inset of Fig. 2. This second resonance therefore arises when the inductive reactance of the nanodipole itself (at a frequency higher than the short-circuit resonance) "goes into resonance" with the air gap capacitance, resulting in large input impedance. The "open-circuit" resonance coincides with the scattering resonant frequency, when the unfed dipole is illuminated by an external plane wave, since the series combination of $Z_{dip}$ and $Z_{gap}$ resonates at this frequency.
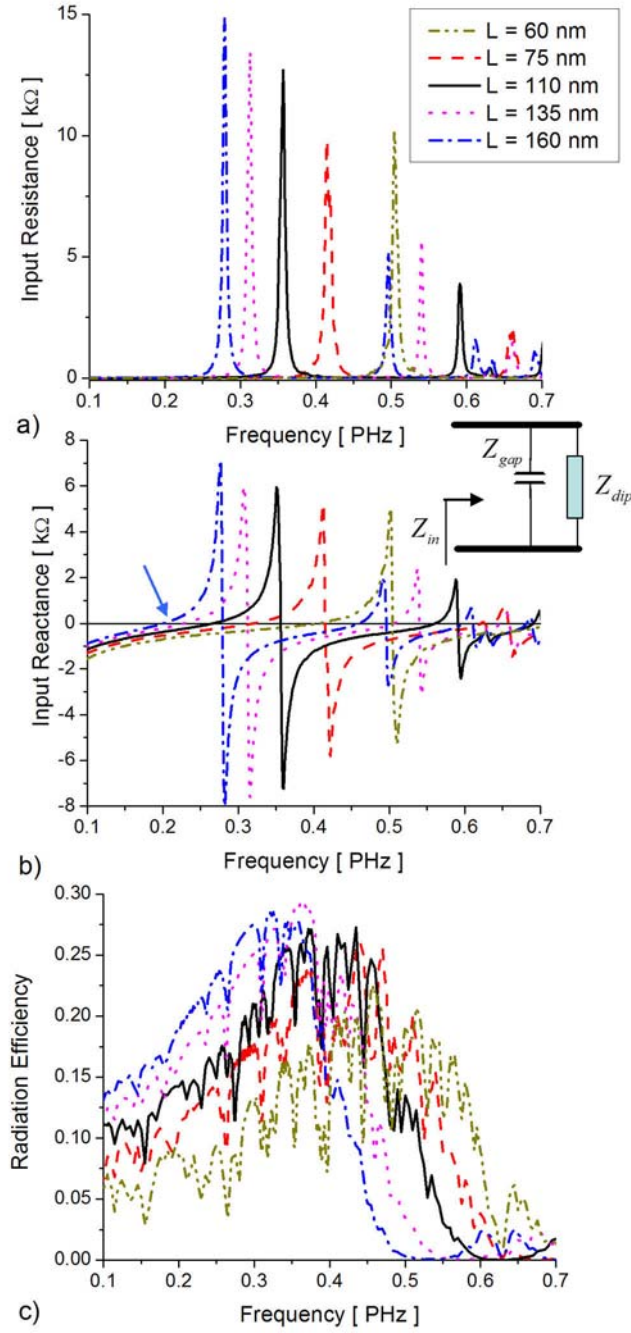
6

Figure 2 – (Color online) (a) Input resistance ($\mathrm{Re}(Z_{in})$), (b) input reactance ($-\mathrm{Im}(Z_{in})$) and (c)

radiation efficiency for the dipole nanoantenna of Fig. 1 made of silver, with $R = 5\,nm$ and

$g = 3\,nm$ varying $L$, calculated numerically using [11].

A regular RF radiating antenna is usually operated at the "short-circuit" resonance for matching reasons, but for the optical nanoantenna operation both these resonant frequencies may be appealing, depending on the impedance of the feeding mechanism (it may be noted that the peak values of input resistance and reactance in Figs. 2a, 2b around the "open-circuit" resonance may be comparable with the characteristic impedance of plasmonic waveguides [13]).

In Fig. 2c, we have evaluated the optical nanoantenna efficiency $\eta_{eff}$, known as the ratio between the total radiated power $P_{rad}$ and the power effectively "accepted" by the antenna input terminals. Although the peak of efficiency is located near the open-circuit resonance, this optical radiation efficiency is reasonably high over a wide frequency window around $L = \lambda_{eff} / 2$, despite the material loss in silver and the nanodipole plasmonic features.

Figure 1 reports the electric and magnetic field distribution in the E plane for a nanodipole with $L = 110\,nm$ at the "short-circuit" frequency $f = 266\,THz$ (at this frequency $\lambda_{eff} \simeq 255\,nm$, slightly larger than the resonance condition $\lambda_{eff} = 2L$, due to the reactive fields at the end of the dipole, which may be approximately taken into account by introducing an effective dipole length $L_{eff} \simeq L + 2R$, consistent with [7]). It is noted that both field distributions resemble those of a conventional half-wavelength resonant RF dipole, ensuring reasonably good radiation and matching at the input port. However, we note the peculiar longitudinal electric field distribution inside the silver dipole, responsible for the flow of optical displacement current along the antenna. This current effectively

plays the role of the conduction current flowing on the surface of an RF dipole made of highly conductive material.

The nanodipole antenna supports other higher-order resonances with different modal distributions around the frequencies for which $L \simeq N \lambda_{eff} / 2$, with $N$ being an integer (the shortening of $\lambda_{eff}$ with frequency is faster than linear, causing a denser increase of modes at higher frequencies). Due to their modal distributions, however, the higher-order resonant modes do not provide a significant far-field radiation, as confirmed by the low radiation efficiency (Fig. 2c) outside the range of frequency for which $\lambda_{eff} \simeq 2L$.

Analogous to the case of RF antennas made of highly conductive metal, for the plasmonic optical nanodipole here we may define an optical radiation resistance as $R_{rad} = P_{rad} / \left(2I_{max}^2\right)$, with $I_{max}$ being the peak of current along the dipole. However, since silver behaves differently at optical frequencies, following our previous discussions in optical nanocircuits [14]-[15] and consistent with Fig. 1a, the current flow along the nanodipole should consider now the flux of optical displacement current, denoted as $-i\omega\varepsilon_{Ag}E_0$, with $E_0$ being the local electric field in silver. In the limit of thin nanodipoles (i.e., $R \ll L$) an approximate standing wave displacement current distribution is expected along the dipole, with expression:

$$I\left(z\right) = I_0 \frac{\sin\left[\frac{\pi}{\lambda_{eff}}\left(L_{eff} - 2|z|\right)\right]}{\sin\left[\frac{\pi}{\lambda_{eff}}L_{eff}\right]},$$
(1)

with $I_0$ being the current entering the nanoantenna arms at the feeding point. The corresponding optical radiation resistance may be evaluated in closed form (not reported here, since it is too lengthy, but plotted in Fig. 3) [16].
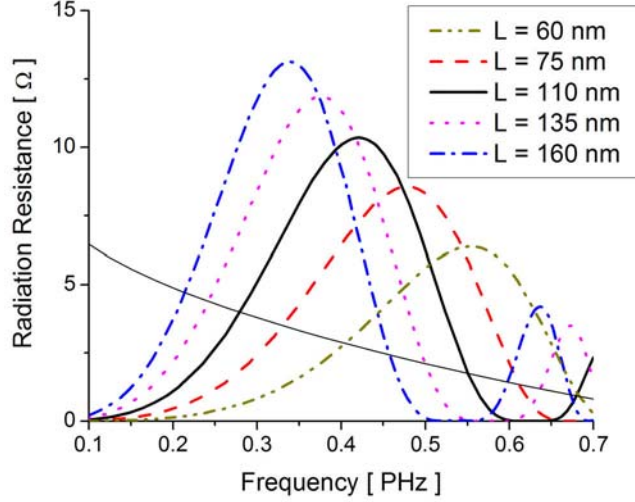


Figure 3 – (Color online) Radiation resistance for the nanodipoles of Fig. 2.

The predicted values of resistance in Fig. 3 are lower, but comparable in magnitude, than those expected from an RF dipole. This effect is due to the shortening of $\lambda_{eff}$ (compared with $\lambda_0$), which leads to an electrically smaller radiation aperture as compared with analogous classic RF dipoles. The thinner solid line in the figure refers to the theoretical radiation resistance evaluated for a nanodipole with $L_{eff} = \lambda_{eff}/2$ (at RF this line would be constant at $73\Omega$). This line crosses the different curves at their corresponding "short-circuit" resonance, validating the numerical results in Fig. 2. At this frequency, $I_{max} = I_0$, implying that the value of radiation resistance in Fig. 3 is "seen" at the input port. Due to the material losses in the nanoantenna, this value is somewhat lower, but comparable in magnitude, than the input resistance at the short-circuit resonant

10

frequency, validating and explaining the numerical results for the radiation efficiency reported in Fig. 2c. The radiation efficiency may in general be given by

$$\eta_{eff} = \frac{R_{rad}}{R_{rad} + \sin^2 x_{eff} R_{loss}} = \frac{R_{rad}}{R_{in}},$$ where $R_{loss}$ is the portion of input resistance

associated with the power lost through absorption in the silver. $R_{rad}$ increases for longer antennas, as seen in Fig. 3, since longer nanodipoles resonate at lower frequencies, for which the effect of wavelength shortening is reduced. This is consistent with the corresponding increase in $\eta_{eff}$ predicted in Fig. 2c.

The above analysis of the nanodipole input impedance allows one to treat the two antenna arms as the "terminals" of a "lumped" element, which in turn would facilitate the design of a feeding waveguide, analogous to what is commonly practiced for conventional RF dipole antennas. This suggests the possibility of designing suitable "nanoloads" for this optical antenna using optical lumped circuit elements in order to adjust and tune the nanodipole resonant frequency or to "match" the nanoantenna with a feeding network at nanoscales. To this end, we "load" the nanodipole of Fig. 1 at its gap region with a nanoparticle (e.g. a nanodisk) made of a material with permittivity $\varepsilon_{load}$, that acts as an optical lumped element [i.e., a nanocapacitor (nanoinductor) when $\mathrm{Re}(\varepsilon_{load})$ is positive (negative)]. In this scenario, the load effectively replaces the air gap and becomes in "parallel" with the antenna terminals, which can still be fed at the gap, for instance by a plasmonic waveguide, as sketched in the inset of Fig. 4 together with the modified circuit model.

11

Figure 4 reports the modification of the input resistance and reactance of the nanodipole, after being loaded with nanodisks of different permittivity. It is evident how the open-circuit resonant frequency may be tuned to the desired value by properly choosing the nanocapacitance or nanoinductance at the gap terminals, without changing the nanodipole length. We point out that this shift in the resonant frequency is not only predictable qualitatively, but it can also be quantified and tailored at will, similar to the antenna design at RF. Following our optical nanocircuit theory [14], the load impedance may indeed be easily evaluated as $Z_{load} = ig/(\omega \varepsilon_{load} \pi R^2)$, being capacitive (inductive) for positive (negative) $\text{Re}(\varepsilon_{load})$.

Since the nanoload is replacing the air gap, it is not surprising to discover that the open-circuit resonant frequency, as obtained in Fig. 4, *quantitatively* coincides with the frequency for which the value of the parallel load reactance $X_{load} = -\text{Im}(Z_{load})$ "goes into resonance" with the dipole's intrinsic reactance $X_{dip} = -\text{Im}[Z_{dip}]$ after proper de-embedding/removing the air gap impedance $Z_{gap}$. The different curves in Fig. 4 may indeed be obtained with very good approximation by considering the parallel combination of the input impedance of Fig. 2 with a capacitance represented by the "additional" parallel load $Z_{add} = (Z_{load}^{-1} - Z_{gap}^{-1})^{-1} = ig/[\omega(\varepsilon_{load} - \varepsilon_0)\pi R^2]$. For instance, when a silicon-nitride nanoload is used in place of the air gap, as seen in Fig. 4, the open-circuit resonance is shifted to $317 THz$, at which $X_{in} = 700\Omega$ from Fig. 2b, and this is

equal to $\mathrm{Im}\left[Z_{add}\right]$ using the above expression. Similar considerations may be verified for the other loads considered in Fig. 4.
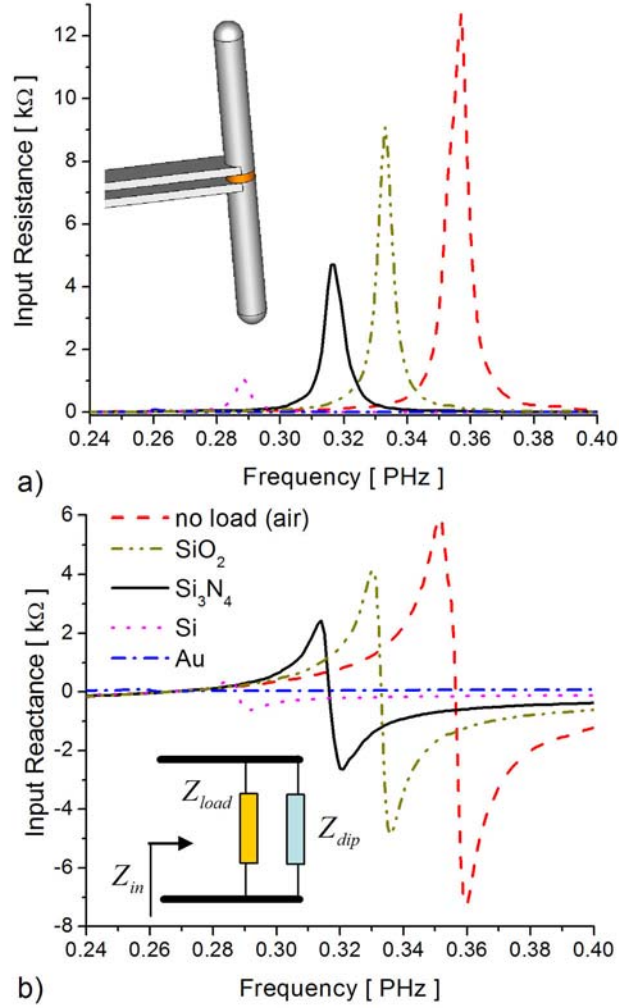


Figure 4 – (Color online) (a) Input resistance and (b) input reactance for the loaded nanodipole antenna of Fig. 1 with $L = 110\,nm$, varying the material of nanoload at its gap.

We also notice that since a larger value of permittivity introduces a larger capacitance for the nanoload, the open-circuit resonance shifts to a lower frequency. By contrast, using a nanodisk made of materials with $\mathrm{Re}\left(\varepsilon_{load}\right) < 0$ (i.e., an inductive load), as it was done by considering a gold nanodisk (blue

curve), shifts the resonant frequency downward to a value below the short-circuit frequency in the region where $X_{dip} < 0$. The "short-circuit" resonance is not modified by the presence of a parallel nanoload, since this resonance is due to the nulling of the intrinsic reactance of the nanodipole without the gap impedance. This resonance may, however, be tuned using a *series* nanoload, placed between the feeding terminals and the antenna arms (not shown here).

The above discussion effectively shows that the concept of nanoantenna loading is analogous to its RF counterpart, when the optical nanocircuit elements [14]-[15] are used to quantify the load impedance. An interesting corollary to this observation is that the input resistance at resonance is consistently reduced, when the permittivity of the parallel nanodisk load is increased (see Fig. 4a), again fully consistent with its circuit model. A judicious design of the parallel loads may allow a good matching between the nanodipole antenna and its feeding system at the open-circuit resonance (e.g., a plasmonic waveguide).

The results presented in this letter may provide an exciting method for tailoring the radiation performance and frequency design of optical nanoantennas and may facilitate the tuning and use of these nanoantennas for various applications in diverse fields such as optical communications, biological and medical sensors at the nanoscales, and nano-optical microscopy.

**References:**

[1] K. B. Crozier, A. Sundaramurthy, G. S. Kino, and C. F. Quate, *J. Appl. Phys.* **94**, 4632 (2003).

[2] P. J. Schuck, D. P. Fromm, A. Sundaramurthy, G. S. Kino, and W. E. Moerner, *Phys. Rev. Lett.* **94**, 017402 (2005).

[3] P. Muhlschlegel, H. J. Eisler, O. J. F. Martin, B. Hecht, and D. W. Pohl, *Science* **308**, 1607 (2005).

[4] J. Aizpurua, G. W. Bryant, L. J. Richter, F. J. García de Abajo, B. K. Kelley, and T. Mallouk, *Phys. Rev. B* **71**, 235420 (2005).

[5] E. Cubukcu, E. A. Kort, K. B. Crozier, and F. Capasso, *Appl. Phys. Lett.* **89**, 093120 (2006).

[6] E. K. Payne, K. L. Shuford, S. Park, G. C. Schatz, and C. A. Mirkin, *J. Phys. Chem. B* **110**, 2150 (2006).

[7] L. Novotny, *Phys. Rev. Lett.* **98**, 266802 (2007).

[8] J. Takahara, S. Yamagishi, H. Taki, A. Morimoto, and T. Kobayashi, O*ptics Lett.* **22**, 475 (1997).

[9] P. J. Burke, S. Li, and Z. Yu, *IEEE Trans. Nanotechn.* **5**, 314 (2006).

[10]    P. B. Johnson, and R. W. Christy, *Phys. Rev. B* **6**, 4370 (1972).

[11]    CST Studio Suite 2006B, www.cst.com.

[12]    C. A. Balanis, *Antenna Theory* (John Wiley & Sons Inc., New York, 1996).

[13]    A. Alù, and N. Engheta, *J. Opt. Soc. Am. B* **23**, 571 (2006).

[14]    N. Engheta, A. Salandrino, and A. Alù, *Phys. Rev. Lett.* **95**, 095504 (2005).

[15]    N. Engheta, *Science*, **317**, 1698 (2007)

[16]    Equation (1) considers the flow of displacement current at the tips of the nanodipole by using the "effective" dipole length $L_{eff} \simeq L + 2R$. Contrary to a conventional RF dipole, here the current at the "physical" tip of the nanodipole is not necessarily zero, since we are considering the *displacement* current as the "flowing" current in the system. With this modification, the standing wave distribution in Eq. (1) describes the displacement current flow along the nanodipole with a good approximation.

[17]    S. Adachi, *Phys. Rev. B* **38**, 12966 (1988).

# 射 频 和 天 线 设 计 培 训 课 程 推 荐

易迪拓培训(www.edatop.com)由数名来自于研发第一线的资深工程师发起成立，致力并专注于微波、射频、天线设计研发人才的培养；我们于 2006 年整合合并微波 EDA 网(www.mweda.com)，现已发展成为国内最大的微波射频和天线设计人才培养基地，成功推出多套微波射频以及天线设计经典培训课程和 ADS、HFSS 等专业软件使用培训课程，广受客户好评；并先后与人民邮电出版社、电子工业出版社合作出版了多本专业图书，帮助数万名工程师提升了专业技术能力。客户遍布中兴通讯、研通高频、埃威航电、国人通信等多家国内知名公司，以及台湾工业技术研究院、永业科技、全一电子等多家台湾地区企业。

易迪拓培训课程列表：http://www.edatop.com/peixun/rfe/129.html

## 射频工程师养成培训课程套装

该套装精选了射频专业基础培训课程、射频仿真设计培训课程和射频电路测量培训课程三个类别共 30 门视频培训课程和 3 本图书教材；旨在引领学员全面学习一个射频工程师需要熟悉、理解和掌握的专业知识和研发设计能力。通过套装的学习，能够让学员完全达到和胜任一个合格的射频工程师的要求…

课程网址：http://www.edatop.com/peixun/rfe/110.html

## ADS 学习培训课程套装

该套装是迄今国内最全面、最权威的 ADS 培训教程，共包含 10 门 ADS 学习培训课程。课程是由具有多年 ADS 使用经验的微波射频与通信系统设计领域资深专家讲解，并多结合设计实例，由浅入深、详细而又全面地讲解了 ADS 在微波射频电路设计、通信系统设计和电磁仿真设计方面的内容。能让您在最短的时间内学会使用 ADS，迅速提升个人技术能力，把 ADS 真正应用到实际研发工作中去，成为 ADS 设计专家…

课程网址： http://www.edatop.com/peixun/ads/13.html

## HFSS 学习培训课程套装

该套课程套装包含了本站全部 HFSS 培训课程，是迄今国内最全面、最专业的 HFSS 培训教程套装，可以帮助您从零开始，全面深入学习 HFSS 的各项功能和在多个方面的工程应用。购买套装，更可超值赠送 3 个月免费学习答疑，随时解答您学习过程中遇到的棘手问题，让您的 HFSS 学习更加轻松顺畅…

课程网址：http://www.edatop.com/peixun/hfss/11.html

## CST 学习培训课程套装

该培训套装由易迪拓培训联合微波 EDA 网共同推出，是最全面、系统、专业的 CST 微波工作室培训课程套装，所有课程都由经验丰富的专家授课，视频教学，可以帮助您从零开始，全面系统地学习 CST 微波工作的各项功能及其在微波射频、天线设计等领域的设计应用。且购买该套装，还可超值赠送 3 个月免费学习答疑…

课程网址：http://www.edatop.com/peixun/cst/24.html

## HFSS 天线设计培训课程套装

套装包含 6 门视频课程和 1 本图书，课程从基础讲起，内容由浅入深，理论介绍和实际操作讲解相结合，全面系统的讲解了 HFSS 天线设计的全过程。是国内最全面、最专业的 HFSS 天线设计课程，可以帮助您快速学习掌握如何使用 HFSS 设计天线，让天线设计不再难…

课程网址：http://www.edatop.com/peixun/hfss/122.html

## 13.56MHz NFC/RFID 线圈天线设计培训课程套装

套装包含 4 门视频培训课程，培训将 13.56MHz 线圈天线设计原理和仿真设计实践相结合,全面系统地讲解了 13.56MHz 线圈天线的工作原理、设计方法、设计考量以及使用 HFSS 和 CST 仿真分析线圈天线的具体操作，同时还介绍了 13.56MHz 线圈天线匹配电路的设计和调试。通过该套课程的学习，可以帮助您快速学习掌握 13.56MHz 线圈天线及其匹配电路的原理、设计和调试…

详情浏览：http://www.edatop.com/peixun/antenna/116.html

## 我们的课程优势：

※ 成立于 2004 年，10 多年丰富的行业经验，

※ 一直致力并专注于微波射频和天线设计工程师的培养，更了解该行业对人才的要求

※ 经验丰富的一线资深工程师讲授，结合实际工程案例，直观、实用、易学

## 联系我们：

※ 易迪拓培训官网：http://www.edatop.com

※ 微波 EDA 网：http://www.mweda.com

※ 官方淘宝店：http://shop36920890.taobao.com